A&A 653, A115 (2021)
https://doi.org/10.1051/0004-6361/202141140
© ESO 2021

Astronomy & Astrophysics

The A-shell star ϕ Leo revisited: its photospheric and circumstellar spectra*

C. Eiroa[1,**], B. Montesinos[2], I. Rebollido[3], Th. Henning[4], R. Launhardt[4], J. Maldonado[5], G. Meeus[6], A. Mora[7], P. Rivière-Marichalar[8], and E. Villaver[2]

[1] Private Researcher, c/ Pablo Casals 20, 28011 Madrid, Spain
[2] Centro de Astrobiología (CAB, CSIC-INTA), ESAC Campus, s/n, 28692 Villanueva de la Cañada, Madrid, Spain
e-mail: bmm@cab.inta-csic.es
[3] Space Telescope Science Institute, 3700 San Martin Drive, Baltimore, MD 21218, USA
[4] Max-Planck-Institut für Astronomie (MPIA), Königstuhl 17, 69117 Heidelberg, Germany
[5] INAF, Osservatorio Astronomico di Palermo, Piazza del Parlamento 1, 90134 Palermo, Italy
[6] Departamento de Física Teórica, Universidad Autónoma de Madrid, 28049 Madrid, Spain
[7] Aurora Technology B.V. for ESA, ESA-ESAC, 28692 Villanueva de la Cañada, Madrid, Spain
[8] Observatorio Astronómico Nacional (OAN,IGN), Calle Alfonso XII 3, 28014 Madrid, Spain

Received 20 April 2021 / Accepted 29 June 2021

ABSTRACT

Context. We previously suggested that variable red- and blueshifted absorption features observed in the Ca II K line towards the A-type shell star ϕ Leo are likely due to solid, comet-like bodies in the circumstellar (CS) environment.
Aims. Our aim is to expand our observational study of ϕ Leo to other characteristic spectral lines of A-type photospheres as well as to lines arising in their CS shells.
Methods. We obtained more than 500 high-resolution optical spectra collected at different telescopes over 37 nights in several observing runs from December 2015 to January 2019. Consecutive time-series spectra were taken, covering intervals of up to ∼9 h on some nights. We analysed some photospheric lines, in particular Ca I 4226 Å and Mg II 4481 Å, as well as the circumstellar shell lines Ca II H and K, the Ca II IR triplet, Fe II 4924, 5018, and 5169 Å, Ti II 3685, 3759, and 3761 Å, and the Balmer lines Hα and Hβ.
Results. Our observational study reveals that ϕ Leo is a variable δ Scuti star whose spectra show remarkable dumps and bumps superimposed on the photospheric line profiles, which vary in strength and sharpness, propagate from blue- to more redshifted radial velocities, and persist for a few hours. Similarly to other δ Scuti stars, these features are likely produced by non-radial pulsations. At the same time, all shell lines present emission at ∼3 km s^{-1} centred at the core of the CS features, and two variable absorption minima at both sides of the emission; those absorption minima occur at almost the same velocity for each line, that is, no apparent dynamical evolution is observed. The variations observed in the Ca II H and K, Fe II, and Ti II lines occur on a range of timescales from minutes to days and between observing runs, but without any clear correlation or recognisable temporal pattern among the different lines. In the case of Hα, the CS contribution is also variable in just one of the observing runs.
Conclusions. We suggest that ϕ Leo is a rapidly rotating δ Scuti star surrounded by a variable, (nearly) edge-on CS disk possibly re-supplied by the δ Scuti pulsations. The behaviour of the CS shell lines is reminiscent of that of rapidly rotating Be shell stars with an edge-on CS disk, and is clear evidence that the variations observed in the CS features of ϕ Leo are highly unlikely to be produced by exocomets. In addition, the observational results presented in this work, together with some recent results concerning the shell star HR 10, highlight the need for critical revision of the Ca II K features, which have been attributed to exocomets in other shell stars.

Key words. stars: individual: ϕ Leo – stars: early-type – stars: variables: δ Scuti – stars: emission-line, Be – circumstellar matter – comets: general

1. Introduction

Transient red- and blueshifted absorption features mainly detected in the Ca II K line towards ∼30 A-type stars have been interpreted as the signatures of the evaporation of large solid, comet-like bodies transiting or grazing the central stars (e.g. Ferlet et al. 1987; Kiefer et al. 2014b; Welsh & Montgomery 2018). This interpretation is reinforced by detections of sporadic events and stable absorptions in some UV metallic lines in the surroundings of a few of those stars, and emission lines at far-infrared (FIR) and (sub)millimetre wavelengths, indicating the presence of secondary cold gas in some debris disk stars. Additionally, photometric observations reveal the presence of exocomets around later type stars (Boyajian et al. 2016; Kiefer et al. 2017; Rappaport et al. 2018); further photometric and spectroscopic evidence for such bodies is found around white dwarf stars (see e.g. Manser et al. 2019; Strøm et al. 2020, and references therein).

Several of the exocomet-hosting A-type stars are known to be shell stars. Those objects, whose CS envelope is most likely a CS disk due to their high rotational velocities ($v \sin i$), have variable, narrow absorption features in many lines of for example

* A copy of the spectra and Table C.1 are only available at the CDS via anonymous ftp to cdsarc.u-strasbg.fr (130.79.128.5) or via http://cdsarc.u-strasbg.fr/viz-bin/cat/J/A+A/653/A115
** Part of this work was made while at the Departamento de Física Teórica of the Universidad Autónoma de Madrid, and as visiting astronomer at Calar Alto Observatory.

Ti II, Fe II, and also the Ca II H and K and IR triplet lines, with the shell lines even appearing and disappearing in some stars (e.g. Jaschek et al. 1988; Abt et al. 1997). However, the similar variable behaviour of the Ca II K line in shell stars and bona-fide cometary-like events detected towards other A-type stars like β Pic or HD 172555 (see e.g. Kiefer et al. 2014a,b) can lead to some misidentification of shell variability (or star binarity) as events from exocomets. A paradigmatic case of this confusion is provided by the shell star HR 10, where the variability of the narrow absorption components superimposed on the photospheric Ca II K line, as well as on Ti II absorption lines at 3759/61 Å, were interpreted as comet-like events caused by infalling comet-like material (Lagrange-Henri et al. 1990; Welsh et al. 1998; Redfield 2007; Abt 2008). However, Montesinos et al. (2019), based on the analysis of a large set of optical spectra spanning several decades, together with interferometric PIONIER/VLTI data, showed that the spectroscopic variations observed in HR 10 are actually caused by its binary nature with CS envelopes around both stellar components.

In the present study, we revisit the shell star ϕ Leo. In a previous paper (Eiroa et al. 2016), we analysed the Ca II H and K non-photospheric CS absorptions and found the most plausible explanation of the observed, striking variability to be comet-like events – although we note that a question mark was included in the title of that paper. However, our analysis of other lines, and numerous time-series spectra taken in 2017 and 2019 and presented here, provide new perspectives about the variability seen in this star, and we now deem our previous analysis to be inappropriate.

The paper is organised as follows: Sect. 2 summarises the properties of the star, Sect. 3 describes the observations, instruments, and observing periods, Sect. 4 describes the results concerning some photospheric and non-photospheric CS lines, with specific examples of spectra obtained in some periods, in Sect. 5 we present a discussion of these results, and Sect. 6 is a brief summary of our conclusions.

2. ϕ Leo: properties

ϕ Leo (HD 98058, HR 4368) is an A5V-A7 IVn shell star (e.g. Jaschek et al. 1991) located at a distance of 56.5 pc. The best stellar parameters, found by Eiroa et al. (2016) from fitting Kurucz photospheric models to high-resolution spectra, are $T_{\rm eff} = 7500$ K, log $g = 3.75$, and $v \sin i = 230$ km s^{-1}, in reasonable agreement with other estimates (e.g. Lagrange-Henri et al. 1990; Royer et al. 2007; Zorec & Royer 2012; Adamczak & Lambert 2014; David & Hillenbrand 2015; Soubiran et al. 2016). Its bolometric luminosity is ~45–50 $L_\odot$ (Zorec & Royer 2012; Adamczak & Lambert 2014; Balona & Ozuyar 2020); the estimated mass is ~2.3 $M_\odot$ (Zorec & Royer 2012; Adamczak & Lambert 2014; De Rosa et al. 2014), while age estimates are in the range ~500–900 Myr (De Rosa et al. 2014; David & Hillenbrand 2015), and the stellar radius has been estimated to be ~3.2 $R_\odot$ with significant oblateness (van Belle 2012; Arcos et al. 2018). ϕ Leo is located in the δ Scuti instability strip of the HR diagram, and has been classified by Balona & Ozuyar (2020) as a δ Scuti variable with several peaks in its TESS periodogram, the strongest one having an amplitude of 5.25 ppt and a frequency of 6.4739 d^{-1}.

Shell Ca II H and K and Ti II 3759, 3761 Å absorption lines have been detected in the spectrum of ϕ Leo (e.g. Abt & Moyd 1973; Jaschek et al. 1988). The shell lines likely arise in a gaseous, close-to-edge-on CS disk given the high rotational velocity of the star (Abt 2008); thus, the triangular shape of the Ca II K profile is probably due to the combination of the photospheric and disk absorptions (Lagrange-Henri et al. 1990). Long-term variations of the Ti II CS lines were reported by Abt (2008), while we found remarkable short-term variations of the Ca II H and K lines (Eiroa et al. 2016). Finally, we note that the star does not possess a detectable warm or cold dusty debris disk (Rieke et al. 2005; Cataldi et al. 2019).

3. Observations

A total of 555 high-resolution spectra of ϕ Leo were collected during ten observing campaigns from December 2015 to April 2017: 389 spectra were obtained with HERMES (Raskin et al. 2011) attached to the Mercator Telescope (La Palma, Spain); 163 spectra with FEROS (Kaufer et al. 1999) at the MPG/ESO 2.2-m telescope (La Silla, Chile); two spectra were obtained with the FIES spectrograph (Telting et al. 2014) at NOT (La Palma, Spain); and one more with CARMENES (Quirrenbach et al. 2016), the high-resolution optical/near-IR spectrograph attached to the 3.5-m telescope at Calar Alto observatory (Almería, Spain). Additionally, 13 spectra were taken in January 2019 with HARPS-N (Cosentino et al. 2012) at TNG (La Palma).

Observing dates, instruments – with their corresponding spectral range and resolution – and the number of spectra per night are given in Table 1; a detailed log with the specific dates and times (UT) is given in Table C.1 of Appendix C. During the 2017 observing runs, ϕ Leo was extensively observed when its airmass was $\lesssim$2; in particular, from March 31 to April 3 the star was continuously followed from La Palma and La Silla for ~9.5 h.

The spectra were reduced using the available pipelines of the corresponding instruments; they include the usual steps for échelle spectra, such as bias subtraction, flat-field correction, cosmic-ray removal, and order extraction. Wavelength calibration is carried out using Th–Ar lamp spectra taken at the beginning and end of each night. Barycentric corrections have been applied to the HERMES, FIES, and CARMENES spectra because the pipelines do not include such correction. Finally, telluric lines have been removed using MOLECFIT, a tool that generates a model atmosphere accounting for the most common absorbing molecules (Smette et al. 2015). Typical signal-to-noise ratios (S/Ns) of the spectra achieved at a continuum of around 4000 Å, that is, close to the Ca II H and K lines, are in the range of ~70–150, mostly depending on weather conditions. The S/Ns of the median spectra of each night are in the range of ~200–500, again depending on weather conditions and the number of spectra per night, and the S/N of the median spectrum of all spectra is ~1000.

4. Results: the spectrum of ϕ Leo

The spectrum of ϕ Leo consists of a broadened A-type photospheric spectrum together with some CS contribution. Figure 1 shows the median spectrum of ϕ Leo in some wavelength ranges with characteristic photospheric Balmer and neutral metallic lines (Fe I, Mn I, Ca I, Na I, O I) of late-type A stars (e.g. Gray & Corbally 2009). This median spectrum has been estimated using all FEROS and HERMES spectra; the latter have been rebinned to the FEROS spectral resolution (0.03 Å pixel^{-1}). The spectra of α Aql and κ Phe, two stars with values of $T_{\rm eff}$ and $v \sin i$ comparable to those of ϕ Leo (Rebollido et al. 2020), are also shown

Table 1. Log of observations.

Observing run	Instrument	Range (nm)	Resolution	Dates (†)	Spectra per night
2015 December	HERMES	~370–900	~85 000	20, 22, 23	1, 4, 1
2016 January	FIES	~370–830	~67 000	26	2
2016 January	HERMES			27, 28, 30	1, 3, 3
2016 March	HERMES			3, 4, 5, 6	4, 4 ,2 ,3
2016 March	FEROS	~350–930	~48 000	25, 26, 27, 28	4, 4, 3, 3
2016 May	HERMES			11	20
2016 May	CARMENES	~520–960/960–1710	~94 600/80 400	19	1
2017 March	HERMES			6, 7, 8, 9, 10, 11, 12, 13	14, 20, 22, 26, 26, 13, 24, 24
2017 March/April	HERMES			28, 29, 30, 31, 1, 2, 3	24, 24, 26, 33, 21, 22, 23
2017 March/April	FEROS			31, 1, 2, 3, 4, 5, 6, 7, 8	8, 28, 26, 11, 16, 16, 13, 16, 15
2019 January	HARPS-N	~392–683	~115 000	29	13

Notes. (†)Dates refer to the beginning of the night; this convention is used throughout the paper.

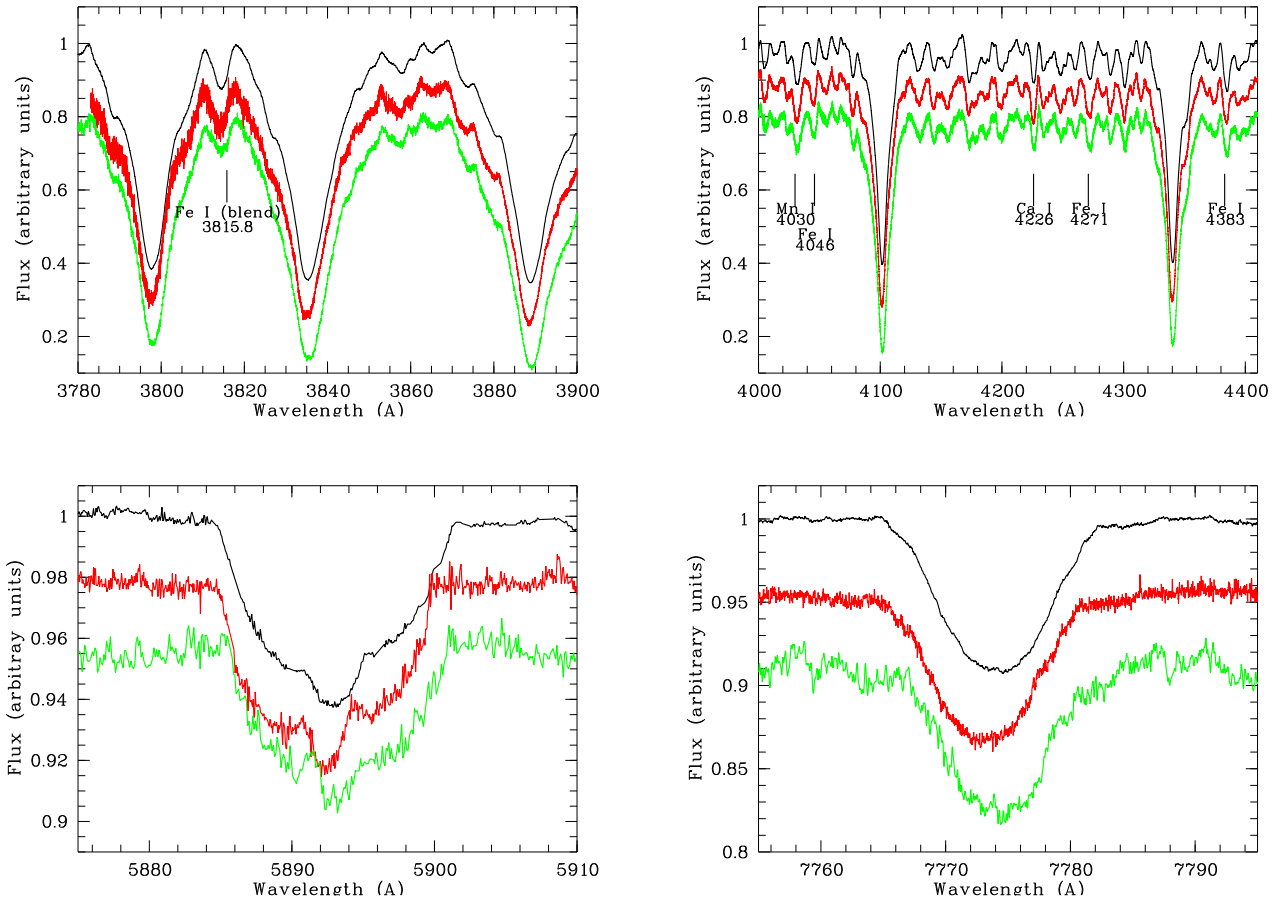

Fig. 1. Photospheric lines of ϕ Leo (black). *Top*: Balmer lines together with some lines due to neutral atoms. The absorption at ~3815 Å is most likely a blend of Fe I lines (the referenced wavelength denotes the strongest Fe I line of the blend, i.e. the one with the highest oscillator strength). *Bottom*: Na II D 5890/96 Å and O I triplet at 7775 Å. For comparison, the spectra of α Aql (red) and κ Phe (green) are also plotted. The strength and width of the Balmer lines and the rest of the spectral features are similar in all three stars, indicating that they are 'pure' photospheric absorptions.

for comparison. The strength and width of the photospheric lines are similar in all three stars.

In addition, ϕ Leo exhibits a number of absorption lines with a clear non-photospheric contribution. Figure 2 shows examples of such lines; in particular the Ca II H and K lines, some Fe II and Ti II lines around the 4481 Å Mg II photospheric one, the Fe II 5169 Å, and the 8542 Å line of the Ca II IR triplet. In this figure, the spectrum of α Aql is plotted directly superimposed on

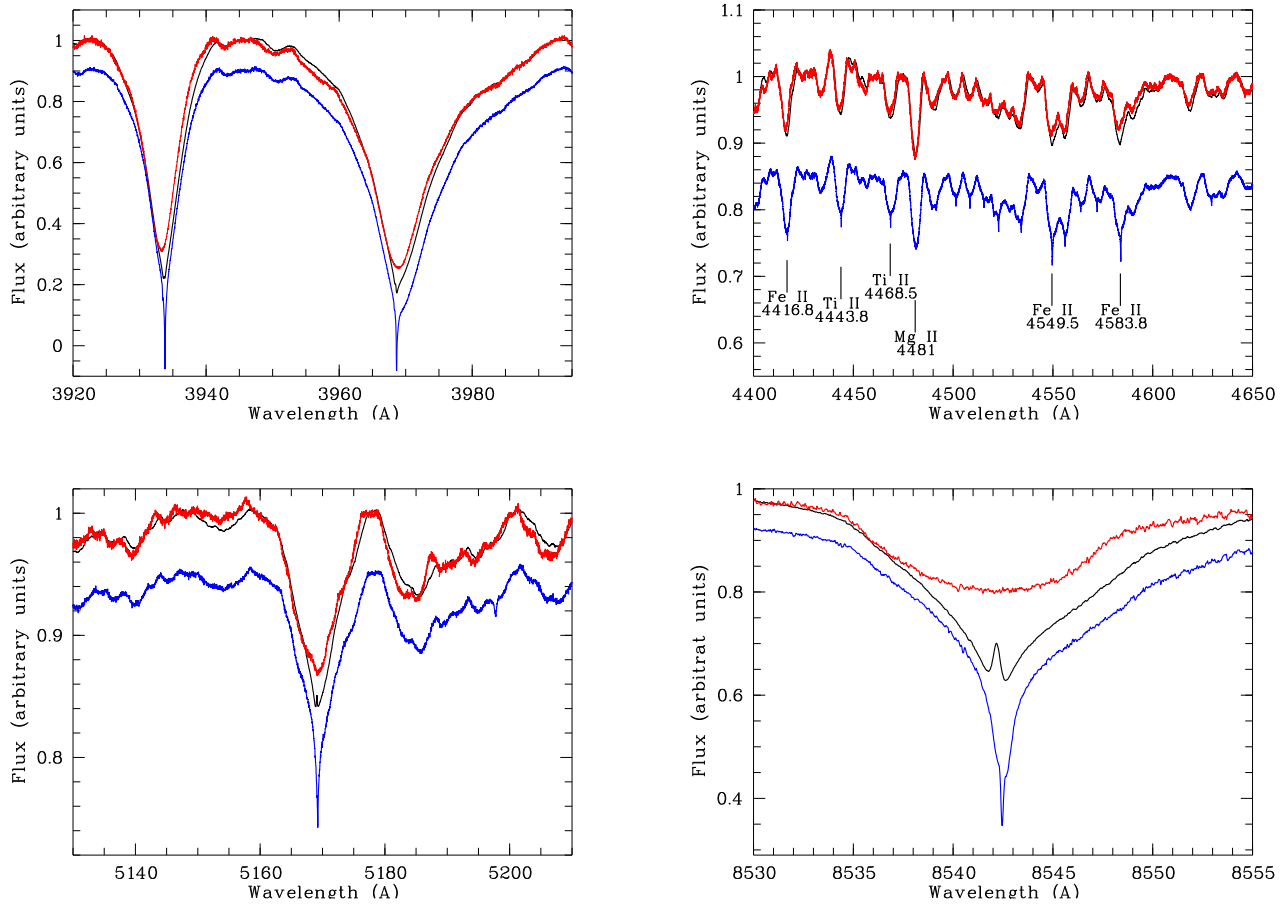

Fig. 2. *Top left*: Ca II H and K lines and the Balmer Hϵ of ϕ Leo (black), together with α Aql (red) and the shell star HR 7731 (blue). The conspicuous non-photospheric contribution in the Ca II lines of ϕ Leo is distinguishable although not as prominent as in HR 7731. *Top right*: same three stars, but in this case the photospheric line Mg II 4481 line is similar in all stars, while the shell Fe II and Ti II lines are striking in HR 7731 but less so in ϕ Leo. *Bottom left*: 5169 Å line of the Fe II triplet 42. *Bottom right*: Ca II triplet line at 8542 Å. The spectrum of α Aql is plotted superimposed on the ϕ Leo spectrum in all panels.

the ϕ Leo spectrum. Figure 2 additionally displays the spectrum of the shell star HR 7731 which also has similar photospheric parameters (Rebollido et al. 2020). We note that the strength of some shell lines in ϕ Leo might be slightly stronger than in α Aql (e.g. the Fe II 4549.5, 4583.8 Å lines) but not comparable with the very strong shell absorptions observed in HR 7731.

ϕ Leo exhibits conspicuous photospheric and circumstellar variability as evidenced by the behaviour of distinctive lines of A-type shell stars. The photospheric line variability becomes discernible as dumps and bumps in the line profiles with similar but not identical characteristics in different lines; careful inspection of several regions close to the photospheric lines shows that such bumps and dumps are not seen in the continuum. The temporal presence of such features is irregular, and when they appear, they usually move from blue to red over short timescales, seemingly lasting for up to a few hours. On the other hand, the CS lines show a common emission at their core, and absorption changes over very short timescales at both the blue and red sides of the core, yet without any apparent correlation among the different lines. In the following two sections we give further details of the photospheric and CS line variability separately.

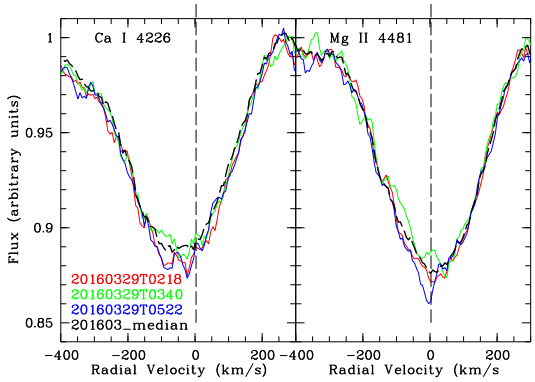

Fig. 3. Ca I 4226 Å and Mg II 4481 Å lines observed with FEROS during the night of 2016-03-28/29. The spectra have been rebinned to a pixel spectral resolution of 6.39 km s^{-1}. The date and UT of each spectrum are indicated. Black dashed line: median of the four-day period shown for comparison. We note the different behaviour of the extra absorption features of each line when compared to their median spectra. The vertical dashed line corresponds to a radial velocity of 3 km s^{-1} (see text in Sect. 4.2 and Fig. 5).

4.1. Photospheric lines

As mentioned above, the median spectrum of ϕ Leo shows photospheric lines typical of a late A-type spectrum (Fig. 1), but individual spectra distinctly show that at least some of those lines (e.g. Ca I 4226.7 Å, Ti II 4468.5 and 4501.3 Å, Mg II 4481 Å, Fe II 4508.3 Å) vary, with the aforementioned

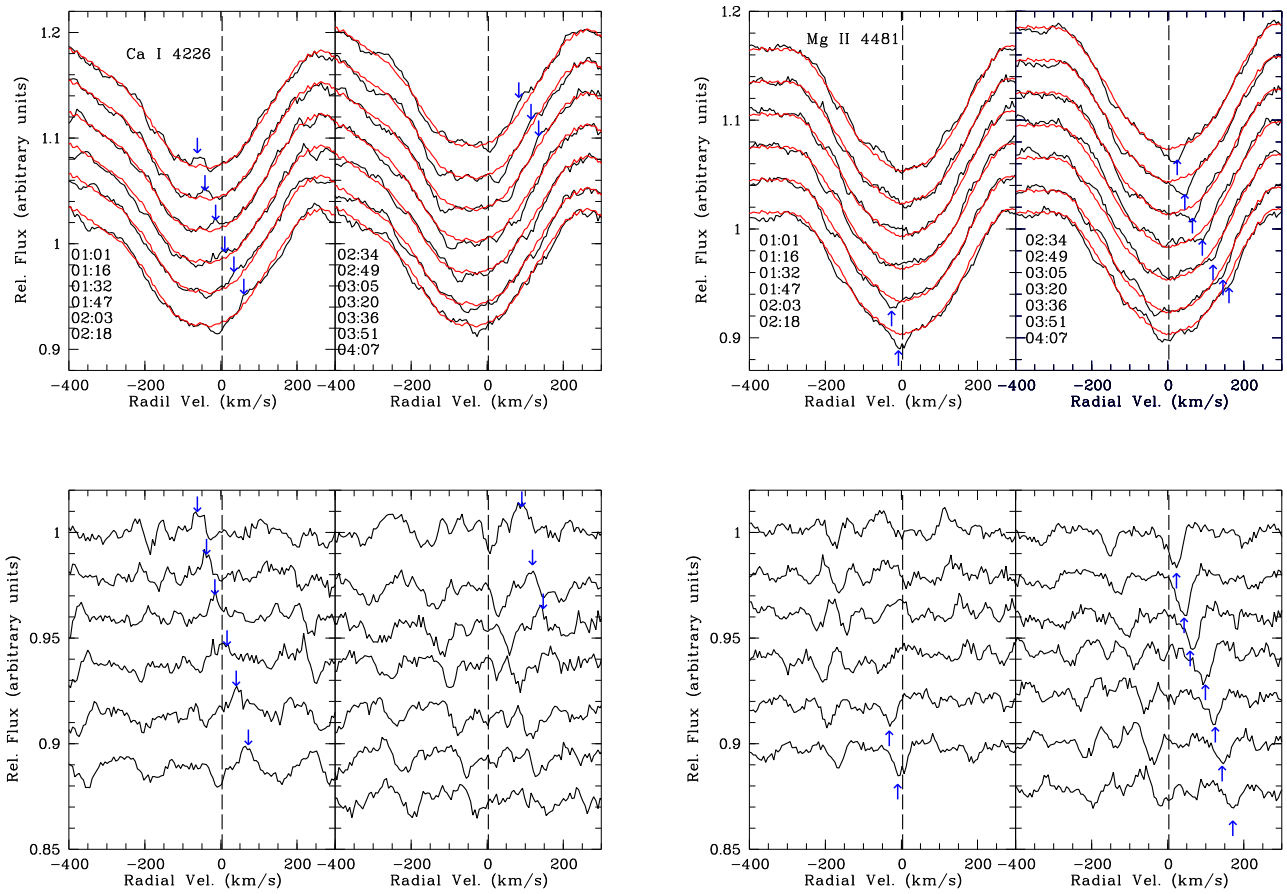

Fig. 4. Ca I 4226 Å and Mg II 4481 Å absorption lines as observed in the 13 consecutive HARPS spectra taken during the night 2019-01-29/30. Exposure time was 15 min per spectrum. The dates and UTs of the spectra are given. Pixel resolution is 5.5 km s^{-1}. The *top panels* show the observed line profiles while the *bottom panels* show the residuals once the median spectrum of the night has been removed. The median spectrum of the night is plotted in red. The blue arrows mark some examples of bumps (in the Ca I panels) and dumps (in the Mg II panels). The black dashed line in all panels corresponds to a radial velocity of 3 km s^{-1} (see text in Sect. 4.2 and Fig. 5).

Table 2. Equivalent widths (mÅ) of Ca I 4226 Å and Mg II 4481 Å during the night 2016-03-28/29.

UT (hh:mm)	Ca I	Mg II
02:18	534	528
03:40	511	501
05:22	550	554
median	530	528

Notes. Estimated uncertainty ~5%.

dumps and bumps appearing superimposed on the line profiles. Figure 3 displays the absorption profiles of the Ca I 4226 Å and Mg II 4481 Å lines, as observed in the three spectra taken with FEROS during the night 2016-03-28/29. Very clear extra absorptions close to the core are observed in comparison to the median spectrum of the whole March 2016 period; the amplitude of variations in the equivalent widths of both lines is small, in the range of two to three times the estimated uncertainties (Table 2).

Time-series spectra taken during the May 2016, 2017, and 2019 observing runs allow us to better characterise the changes in the absorption lines, and to trace their temporal evolution with a time resolution of between 4 and 15 min during a time interval from ~3 up to ~9 hours (during some nights of March-April 2017, HERMES and FEROS spectra were consecutively collected for a time interval of ~9.5 h; some spectra were even obtained simultaneously using both telescopes). Figure 4 shows the profile of the Ca I 4226 Å and Mg II 4481 Å lines corresponding to the 13 consecutive spectra obtained with HARPS-N in January 2019 during ~3 hours of observations; the integration time of each spectrum was 15 min. Several dumps and bumps propagating across the profile at different radial velocities can be distinguished; in both lines the features vary their radial velocity at a rate of ~100 km s^{-1} per hour (to guide the eye some of them are marked with arrows in the figure). Figure 4 shows the median of the HARPS-N spectra superimposed on each observed individual spectrum as well as the residuals once the median spectrum has been removed. The features (dumps and bumps) propagate towards redder velocities, first increasing their strength, achieving a maximum at a velocity of ~3 km s^{-1}, which is close to the apparent emission detected in CS features (see details in Sect. 4.2 and Fig. 5), and then decreasing their strength, for seemingly ~1 to ~3 h; their persistence from profile to profile suggesting that they are real and not artifacts or noise. Similar features, varying their strength and sharpness, and moving from blueshifted to more redshifted velocities, superimposed on the median line profiles are seen in other nights. We note that the time-span, velocity interval, and maximum strength are irregular, and that the behaviour of the Ca I and Mg II

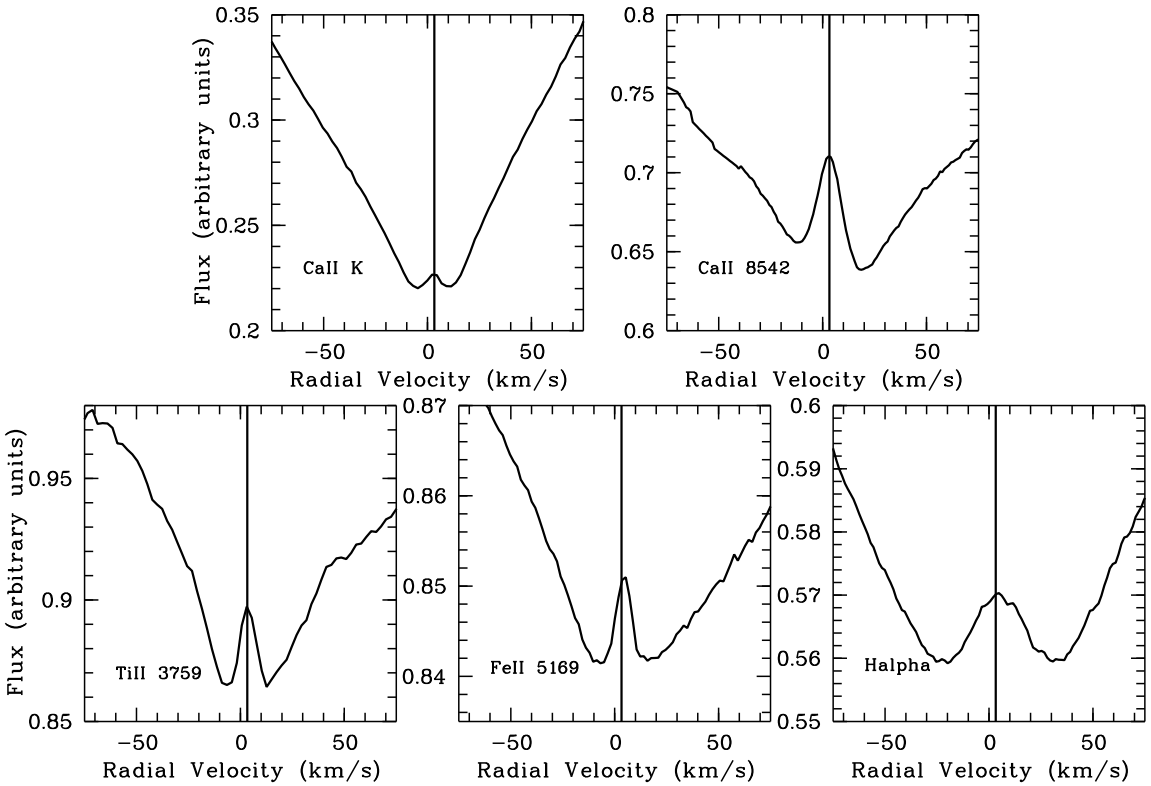

Fig. 5. Line profiles in velocity units of metallic absorptions showing a clear non-photospheric contribution. Hα is also plotted. The profiles correspond to the median of all ϕ Leo HERMES and FEROS spectra. The vertical line corresponds to a radial velocity of 3 km s^{-1}. In the case of the Ca II K line, the profile corresponds to the 'pure' CS contribution, i.e., the photospheric absorption has been removed (see text).

lines is not quite coincident, or in other words, the variations do not seem to be in phase. The fact that they do not correlate might suggest that the lines originate from different layers in the stellar photosphere. We also note that dumps and bumps are not always clearly present in many of the spectra. Appendix A presents some further spectra of the Ca I 4266 Å and Mg II 4481 Å photospheric lines.

4.2. Circumstellar absorptions

Prominent non-photospheric shell-like features are seen in the Ca II H and K lines, the Ca II triplet at 8498, 8542, and 8662 Å, the Ti II lines at 3685, 3759, and 3761 Å, the Fe II triplet at 4923.9, 5018.4, and 5169 Å, and the Balmer lines Hα and Hβ. Other shell lines, such as those observed in other shell stars (see e.g. the spectrum of HR 7731 shown in Fig. 2) are either hardly distinguishable or undetected. Figure 5 shows the median HERMES and FEROS spectrum in velocity space of some of those lines; in the case of the triplet lines the most representative one is shown. These lines show common and distinct behaviours:

(i) The median spectrum of the non-photospheric metallic features shows prominent emission at the line centre (Fig. 5). The emission peak is located at a velocity of ∼3 km s^{-1}. The emission at the core is also present in the Hα line and very weak in Hβ. We note that the emission in the Ca II H and K lines is not apparent in the 2015 spectra (see Fig. 6) but it clearly appeared in the 2017 and 2019 spectra, as well as in the 2016 spectra (see Fig. 7). In Figs. 6 and 7, the photospheric line contribution has been removed; the procedure we followed to visualise the Ca II H and K CS features is described below after item (v);

(ii) Manifest variability is observed in the Ca II H and K and Fe II triplet lines, together with less pronounced variations in the Ti II lines. Changes are observed on various timescales ranging from minutes to days and between observing runs, as perceived when comparing spectra taken during the same night, or the median spectra of the different nights or observing periods. The variations do not show a discernible temporal pattern, and there is no correlation between the observed variability of the different metallic ions;

(iii) As in the metallic lines, an absorption excess is clearly visible at the core of Hα (Fig. 8). Hα and Hβ remained free of any noticeable changes in the spectra taken with HERMES and FEROS from 2015 December to 2017 April, but Hα displayed clear variability in the spectra of 2019-01-29 taken with HARPS-N. These variations do not exactly correlate with those simultaneously observed in the Ca II and Fe II lines;.

(iv) The Ca II triplet lines do not show any apparent change when spectra are compared on any timescale. However, we note that the HARPS-N spectra do not cover these lines; therefore, we do not know if these lines varied in 2019-01-29 as Hα did;

(v) In all CS lines, including Hα, the variability shows up as changes in the relative absorption strength at both blue and red minima of the central emission, but the strength of those minima in the median spectrum is almost indistinguishable (Fig. 5). In the case of the constant Ca II triplet lines, the blue side is always weaker than the red side. Further, the minimum appears at nearly the same radial velocity for all lines.

Spectra of some observing runs that illustrate the mentioned points above are shown in the following sections. Beforehand, we point out that, in the case of the Ca II H and K lines, the plots show the CS features once the photospheric contribution

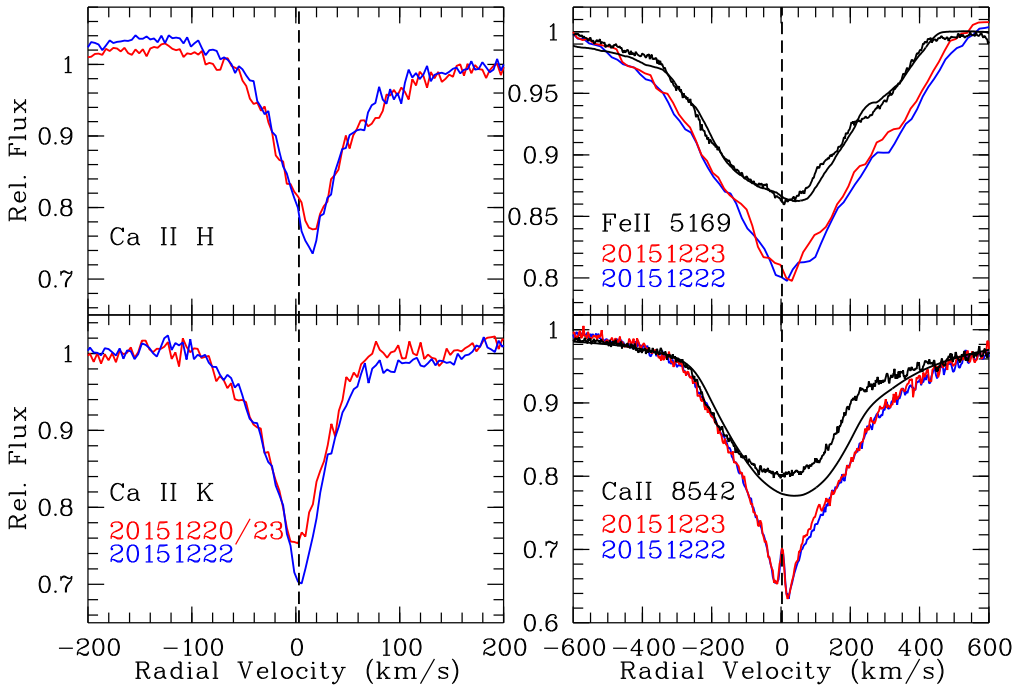

Fig. 6. *Left*: Circumstellar Ca II H (up) and K (bottom) features of the HERMES spectra taken in December 2015. The photospheric line has been removed as estimated from Kurucz synthetic models (this is the procedure followed for all Ca II H and K plots, see Sect. 4.2). The spectra have been rebinned to 3 pixels (size 3.56 km s^{-1}). *Right (bottom)*: Ca II 8542 Å. The spectra have been rebinned to a resolution of 3.29 km s^{-1} per pixel. Right (up) Fe II 5169 Å line; the pixel resolution in this case is 8.16 km s^{-1}. The photospheric contribution is not removed in the right panels (this is the procedure for all plots of these lines). Dates are colour-coded. The vertical dashed line corresponds to a radial velocity of 3 km s^{-1} (this line is plotted in all plots). For comparison, and to visualise the CS contribution, the right panels also show in black the Fe II 5169 Å and Ca II 8542 lines of the ϕ Leo Kurucz model and the observed spectrum of the star α Aql.

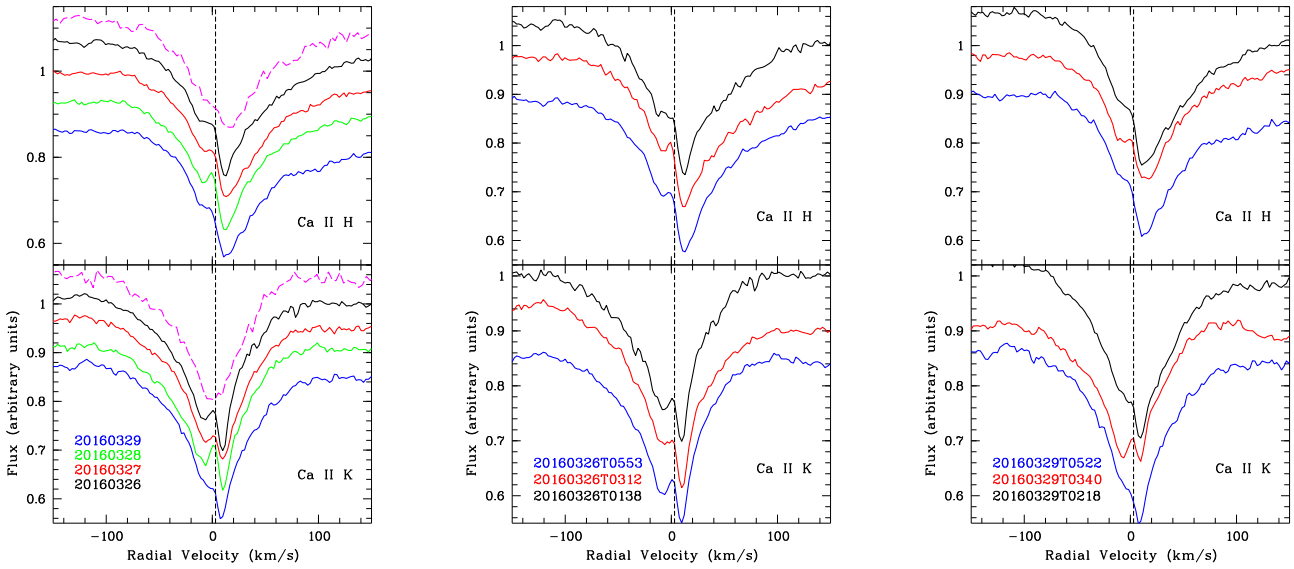

Fig. 7. Ca II H and K spectra taken with FEROS during March 2016. The left panel plots the median of all four nights, while the middle and right panels show the observed features on two different nights. The UTs are indicated in the labels. For comparison, the 2015-12-20/23 spectrum is shown in the left panel (dashed lines).

has been removed. This is carried out by dividing the observed profiles by synthetic ones estimated using the Kurucz synthetic spectrum computed with the T$_{\rm eff}$, log g, and $v \sin i$ values of Sect. 2 as it provides a very reasonable fit; see Fig. 1 in Eiroa et al. (2016). We are aware that because of the high rotational velocity, the oblateness of ϕ Leo, as mentioned in Sect. 2, could be significant, and therefore a gradient from equator to poles in at least $T_{\rm eff}$ and log g must be present due to gravity

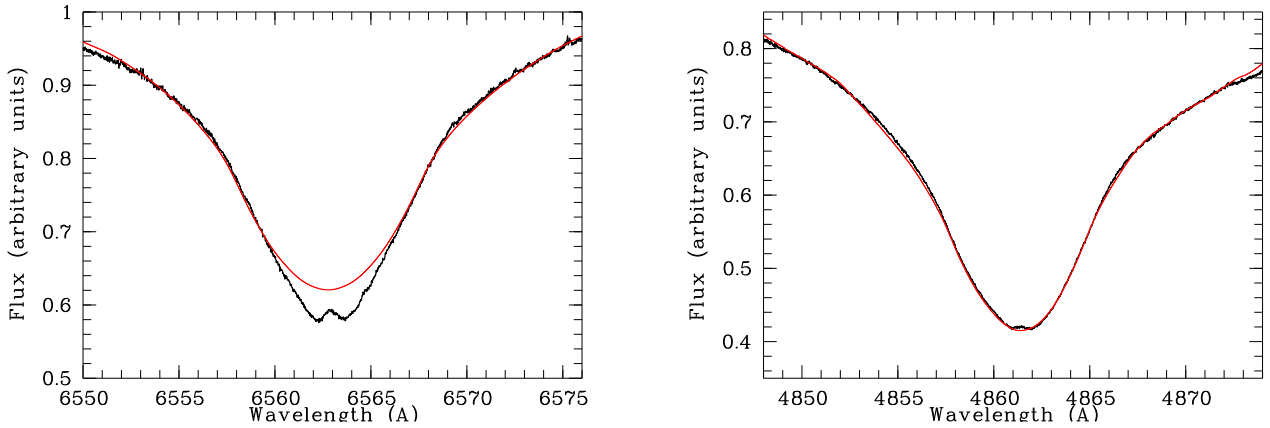

Fig. 8. Median profiles of the Hα and Hβ lines taken with HARPS with the Kurucz model superimposed.

darkening. Nonetheless, we are confident that our estimates provide reasonable mean values because our Kurucz model for α Aql gives a very good fit (see Fig. 1 of Eiroa et al. 2016), this star also being affected by gravity darkening because of its relevant oblateness (e.g. Bouchaud et al. 2020).

4.2.1. HERMES December 2015

The Ca II H and K lines of December 20 and 23 are similar, showing a broad non-photospheric absorption in addition to the photospheric line (see e.g. Fig. 1 by Eiroa et al. 2016); at the same time, the four spectra of December 22 remain constant, and the absorption at the core is deeper than in the other two nights. Based on this result, and on the behaviour of other spectra obtained in 2016, Eiroa et al. (2016) assumed that the spectra of December 20 and 23 represented a stable absorption formed by the contribution of the stellar photosphere and a CS gas disk, which was taken as a template to analyse other contributions and/or variations to the CS gas. However, the detection of the central 3 km s^{-1} emission in the spectra of 2017 and 2019, which was not clearly present in 2015, provides a new perspective, indicating that the assumption in our previous work (Eiroa et al. 2016) was not appropriate. We now note that the depths in the December 22 spectra are among the deepest absorptions of all spectra taken in different observing runs, and that the December 20 and 23 spectra have depths similar to many other spectra. Also, the profile of the CS Ca II H and K absorption in December 2015 suggests that the 3 km s^{-1} emission at the core was hidden or not present. Thus, our analysis is now carried out considering the whole absorption in excess of the photospheric line given by our Kurucz model.

Figure 6 (left) shows the nightly average of the non-photospheric Ca II H and K features once the photospheric line has been removed. It can be observed that both Ca II H and K features are deeper in December 22 than in December 20 and 23. The estimated equivalent widths of the K/H features are ~227 mÅ/~234 mÅ and ~249 mÅ/~245 mÅ, for the spectra December 20 and 23 and December 22, respectively; these figures suggest that the Ca II features are saturated. The peak of the K absorption is centred at the velocity of the 3 km s^{-1} central emission, although, as pointed out above, such emission is not present in these spectra, and the H line appears at a velocity of ~15 km s^{-1}. Such a shift to more redshifted velocities is observed in other shell stars (Rebollido et al. 2020), and is likely due to the influence of the Hϵ line. Figure 6 (right) also shows the Fe II 5169 Å and the Ca II 8542 Å lines, where one can appreciate that Ca II 8542 Å does not vary and clearly shows the central 3 km s^{-1} emission, while the Fe II line does not vary appreciably (i.e. it differs in behaviour from the Ca II H and K lines) and the central emission is not present. The Balmer Hα and Hβ lines (not shown) are constant and present the 3.0 km s^{-1} central emission.

4.2.2. FEROS March 2016

Figure 7 shows the Ca II H and K CS features as observed in this period once the photospheric contribution has been removed. Variability can be observed on a nightly basis as well as in the median of each of the four observed nights; we see that, unlike the procedure followed by Eiroa et al. (2016), the 3 km s^{-1} emission feature is distinctly distinguishable in many of the individual and median spectra. For comparison, the feature as observed in 2015-12-20/23 is also plotted in the figure. In this way, it is easy to see that the variable absorption at both blue- and redshitfted sides of the central emission can be mistaken for FEB events similar to those of β Pic, if, as assumed by Eiroa et al. (2016), the 2015-12-20/23 feature is taken as a stable template. Additionally, we point out that the variations in the strength of the CS absorption at both blue and red sides of the central emission is recursive in other observing runs; that the changes do not follow an identifiable temporal pattern; and that the velocity of the blue and red deepest absorptions is always similar: $\sim -10/-6$ km s^{-1} and $\sim 10/20$ km s^{-1}, respectively.

Figure 9 plots the Fe II 5169 Å and the Ti II 3759 and 3761 Å lines. In the case of the Fe II line, we have chosen to show the median spectra of each night, while in the case of the Ti II lines the median spectra as well as the individual spectra of the night 26/27 March are plotted. The 3 km s^{-1} emission is seen in all cases, and is particularly conspicuous in all spectra of both Ti II lines. As in the case of the Ca II K line, changes in the strength of the lines at both sides of the central emission are observed, but without any clear correlation among the variations in the different lines. We briefly mention that there are no identifiable changes in the Balmer and Ca II triplet lines.

4.2.3. HARPS-N January 2019

Figure 10 shows the Ca II K, Fe II 5169 Å, and Hα as observed in the 13 consecutive spectra taken with HARPS during the night of 2019-01-29/30, with an exposure time of 15 min each, the first

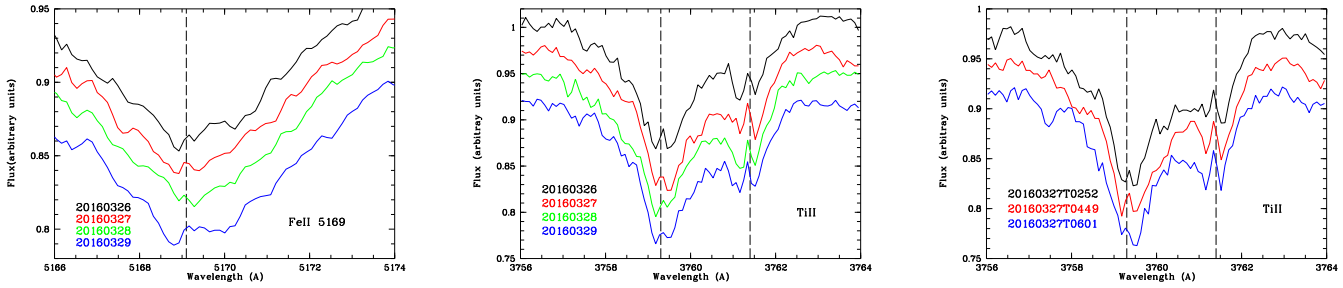

Fig. 9. *Left:* Fe II 5169 Å median daily spectra taken with FEROS during March 2016. *Middle:* median daily spectra of the Ti II lines 3759 and 3761 Å. *Right:* same Ti II lines as observed in the night 2016-03-26/27. Resolution is 1.2 Å pixel^{-1}. UTs are indicated in the labels. In all plots, the dashed line corresponds to a 3 km s^{-1} velocity.

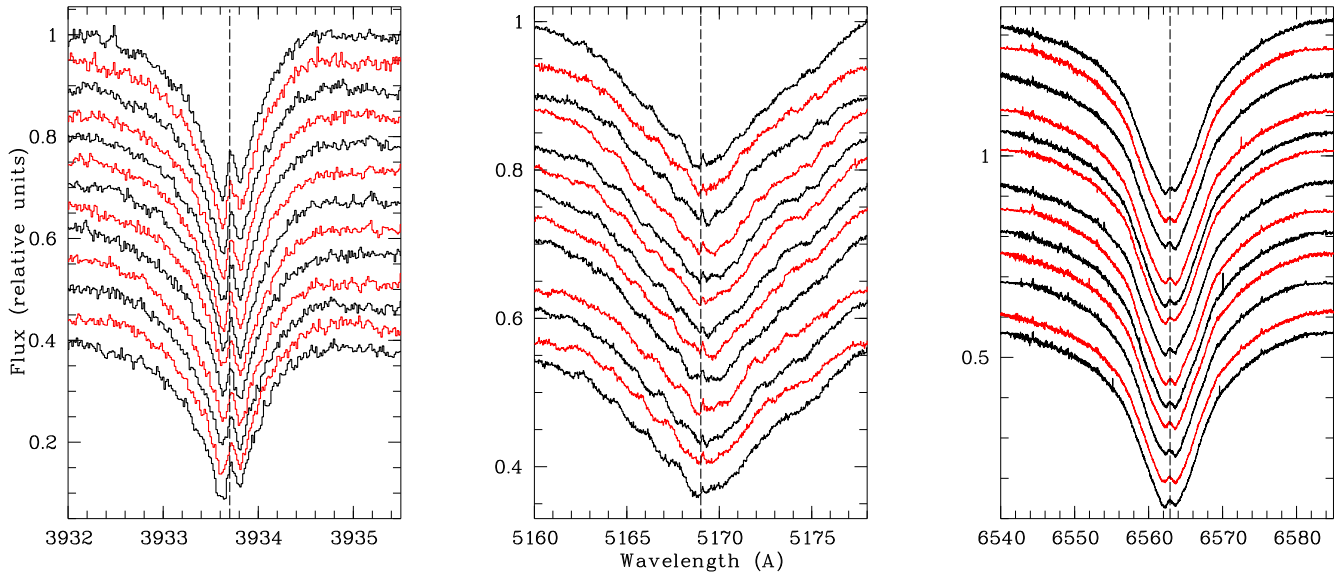

Fig. 10. Ca II K (*left panel*, resolution 0.016 Å pixel^{-1}), Fe II 5169 Å (*middle*, resolution 0.03 Å pixel^{-1})), Hα (*right*, resolution 0.01 Å pixel^{-1}). Spectra were taken with HARPS-N during the night of 2019-01-29/30; each spectrum is 15 min apart starting 01h01m UT (first spectrum at the top) and finishing 04h07m UT (last spectrum at the bottom). The dashed line corresponds to a velocity of 3 km s^{-1}.

at the top starting at 2019-01-30 01h01m UT. The photospheric contribution has been removed in the case of the Ca II lines. The central emission is clearly visible in all Ca II and Hα spectra, but it is not as obvious in the case of some Fe II line profiles. Variability is seen at both sides of the central emission among the individual consecutive spectra in all three lines; again that variability does not follow a regular temporal pattern, and there is no correspondence in the variability of the different lines. We note, as in previous spectra of other observing runs, that the blue and red absorption peaks occur at almost the same velocity without any evolution in this regard.

5. Discussion

5.1. The δ Scuti photosphere

The temporal variation of the photospheric lines and the δ Scuti TESS photometric variability (Balona & Ozuyar 2020) are alike. As stated in Sect. 2, ϕ Leo is most likely seen edge-on; therefore, assuming a stellar radius of 3.2 $R_\odot$ and 230 km s^{-1} as the equatorial velocity, the rotation period would be $P \approx 17$ h, which is seemingly larger than the apparent temporal duration of the features crossing the photospheric lines. While the uncertainty of the assumed stellar parameters is high, because this estimate does not take into account the oblateness of the star, and consequently the expected gravity darkening, and assumes an edge-on inclination, it does nevertheless suggest that the observed bumps and dumps in the line profiles are not modulated by rotation, which also argues against the existence of spots on the surface of the star. Similar temporal behaviour of bumps and dumps crossing the profiles of photospheric lines from blue to red on timescales of hours has been seen for several decades in other δ Scuti stars (Walker et al. 1987; Kennelly et al. 1992, 1998; Balona 2000; Mantegazza 2000), as well as in Be stars (e.g. Vogt & Penrod 1983; Baade 1984; Kambe et al. 1993a,b; Leister et al. 1994), and early-type supergiants (e.g. Baade & Ferlet 1984). The common interpretation is that non-radial (longitudinal) pulsations are caused by motions along longitudinal strips; those non-radial pulsations divide the stellar surface into regions with different velocity fields, which, in the presence of rotation, redistribute the flux over the absorption line profile to create moving patterns of peaks and troughs (e.g. Walker et al. 1987; Telting & Schrijvers 1997; Schrijvers & Telting 1999; Mantegazza 2000; Telting 2003, and references therein). The non-radial pulsations can even be related to stellar rotation in the sense that rapid

rotation facilitates the detection of this kind of pulsation (Baade & Ferlet 1984). A deeper analysis of the spectroscopic photospheric variability in conjunction with the TESS photometric data is deferred to another work.

5.2. The circumstellar disk

The common feature shared by the detected CS absorptions mentioned in Sect. 4.2 is the ∼3 km s^{-1} emission at the core of the lines. We have checked the spectra of all shell stars – 18 objects – included in the sample of Rebollido et al. (2020) and no comparable spectral characteristic is present, with the exception of a similar stable Ca II triplet profile with weaker emission at the centre and the blue side than the red side in the stars HD 21688, HD 39182, and HD 42111. In the case of HD 21688, emission is also observed in the centre of the Hα line, while HD 39182 and HD 42111 display complex Fe II 5169 Å profiles. At the same time, the shape of the Ca II triplet in HD 85905 is similar to the shape in these stars, but its radial velocity changes remarkably as it happens in other shell lines, while the photospheric lines remain constant. Further, we note that all the previously mentioned stars, with the exception of HD 21688, have variable Ca II H and K CS features, and other shell stars with variability in these Ca II lines in Rebollido et al. (2020), namely HD 256 (HR 10), HD 37306, HD 50241, HD 138629, HD 148283, and HD 217782, have single narrow shell absorptions. Thus, the emerging picture of the A-type stars with CS shells is the one of a heterogeneous class of stars, which merely reflects previously known results (e.g. Jaschek et al. 1988; Jaschek & Andrillat 1998).

Interestingly, similarly to the CS shell line profiles in ϕ Leo, central emission at the core of shell lines with two absorption minima at both sides is also observed in the rapidly rotating Be shell stars (e.g. Rivinius et al. 1999). Such 'central quasi emission' (CQE) peaks are non-photospheric because they are only observed in shell lines (Koubsky et al. 1993, 1997), and are favoured by the presence of an edge-on CS disk, which should be optically thin in the continuum, have a small spatial extent, and show little line broadening (Hanuschik 1995; Rivinius et al. 1999). We note here that ϕ Leo is also a rapidly rotating star with a plausible edge-on CS disk. Central quasi emission results from the local minimum at zero radial velocity in the fraction of the stellar disk occulted by CS gas in Keplerian orbital motion, that is, gas moving perpendicular to the line of sight, as predicted in Hanuschik's Keplerian model for CS disks around Be shell stars; thus, CQE is a pure absorption phenomenon – occurring at a few stellar radii – not related to any emission process (Hanuschik 1995; Rivinius et al. 1999). Following the model by Hanuschik (1995), we can estimate the radius of the ϕ Leo CS disk ($R_{\rm abs}$) where the shell absorption lines form; thus, using Eq. (1) in Rivinius et al. (1999), namely $R_{\rm abs} = (\Delta v_{\rm cusps}/2v_{\rm crit} \sin i)^{2/3}$, where $\Delta v_{\rm cusps}$ is the velocity separation of the two minima around the CQE, and $v_{\rm crit}$ is the critical velocity of the star ($v_{\rm crit} = (GM_\star/R_\star)^{0.5} \simeq 370$ km s^{-1}, assuming the values of $M_\star$, $R_\star$ given in Sect. 2 for ϕ Leo, and considering only the centrifugal and gravitational forces), we obtain $R_{\rm abs}$ equal to ∼13.5 $R_\star$ for the Ca II K line, ∼10.7 $R_\star$ for Ti II 3759 Å, ∼9.8 $R_\star$ for Fe II 5169 Å, ∼8.5 $R_\star$ for Ca II 8542 Å, and ∼5.7 $R_\star$ for Hα. We note that these values of $R_{\rm abs}$ are similar to those estimated by Abt et al. (1997) for the Ti II lines assuming a Keplerian scenario. Variability in the strength of the absorption minima at both sides of the CQE, similar to the changes observed in ϕ Leo, are also known to be exhibited by some Be shell stars, for example ϵ Cap (see Fig. 3 in Rivinius et al. 1999); such changes might be due to the re-supply of matter from the star to the disk. Mechanisms for sufficient angular momentum transfer from the star to the disk in Be stars are a matter of debate (e.g. see Rivinius et al. 2013); among them, the more firmly established are those relating the disk and stellar non-radial pulsations (e.g. Cranmer 2009, and references therein). Given the plausible evidence for the presence of this kind of pulsation in ϕ Leo provided by the spectroscopic variations of its photospheric lines, it is tempting to hypothesise that such a mechanism could also be at work in this star.

We also note that the absorption minima at both sides of the central emission always show up at similar radial velocities for each line, but they are different for each one, without any apparent dynamical evolution, making them different from the bona-fide exocometary events observed in β Pic. This fact, together with the variability and changes observed in the lines of Ca II, Fe II, and Ti II from almost one spectrum to the next, and on a range of timescales, suggests that such line variations in ϕ Leo are highly unlikely to be produced by comet-like bodies.

5.3. A brief note on the exocomet-host shell stars

As indicated in Sect. 1, around 30 stars have been suggested to host exocomets in their immediate surroundings based, for the most part, on the variable events observed in the Ca II K line. Among those 30 stars, 10 are A-type shell stars, including ϕ Leo and HR 10; see Table 7 in Rebollido et al. (2020). However, the HR 10 results presented by Montesinos et al. (2019) and those of ϕ Leo presented here, in both cases based on a very large amount of observational data, clearly demonstrate the need for a deeper analysis of the stellar spectra (at least in the shell stars), extending to large periods of time and to the behaviour of other shell lines, and not restricted to the Ca II K line. For instance, we note that Rebollido et al. (2020) pointed out in the case of the shell star HD 85905 that the observed spectral variations could be due to variability of the CS shell as suggested by the observed changes of several shell lines, and not just the Ca II K line; further, we note in the previous section the similar or dissimilar behaviour of different lines among shell stars that appears to be independent of the variability of the Ca II K line.

6. Conclusions

Our spectroscopic observations reveal that ϕ Leo is a highly variable δ Scuti type A-shell star with remarkable changes in its photospheric and CS lines. The photospheric variability manifests as dumps and bumps superimposed on the line profiles, varying their strength and sharpness and propagating from blue- to more redshifted radial velocities; those features persist for a few hours, with a timescale of the order of the δ Scuti photometric variations observed with TESS (Balona & Ozuyar 2020). Thus, similarly to other δ Scuti stars, the ϕ Leo spectroscopic photospheric variability is likely produced by non-radial pulsations caused by motions along longitudinal strips on the stellar surface.

Regarding the non-photospheric CS lines, our data suggest that ϕ Leo is a late A-type star, whose shell is a disk seen nearly edge-on, and with characteristics reminiscent of the ones observed in Be shell stars. Thus, we are faced with the case of a relatively late-spectral-type star, with a consequently relatively low mass, exhibiting a Be shell-like phenomenon. In summary, ϕ Leo is plausibly a rapidly rotating δ Scuti star surrounded by a variable CS disk that is possibly re-supplied by the δ Scuti

pulsations. To our knowledge, theoretical efforts focusing on such a scenario have been limited to B stars but not to late-type A stars (e.g. Rivinius et al. 2013, and references therein); in this respect, ϕ Leo provides an incentive to extend such studies to less massive stars. Finally, we find that this CS scenario for ϕ Leo is more plausible than the exocomet scenario first suggested by Eiroa et al. (2016); the central emission, together with the variable absorption minima at both sides – changing their strength but not their velocity – in the lines of Ca II, Fe II, and Ti II, which also show variability from almost one spectrum to another, and in some periods also in Hα, are highly unlikely to be produced by comets.

Finally, the observational results presented in this work, together with those presented by Montesinos et al. (2019) concerning the shell star HR 10, suggest the need for a critical revision of hypotheses regarding the origin of the variable features in the Ca II K line observed in other shell stars, which thus far have been attributed to exocomets.

Acknowledgements. The authors thank the referee for the comments and suggestions to the original manuscript. This work is based on observations made at the Spanish Observatorio del Roque de los Muchachos (La Palma, Spain) of the Instituto de Astrofísica de Canarias with the Mercator Telescope, operated by the Flemmish Community, the Nordic Optical Telescope, operated by the Nordic Optical Telescope Scientific Association, and the Italian Telescopio Nazionale Galileo (TNG) operated by the Fundación Galileo Galilei of the INAF. Based on observations made with the ESO/MPG 2.2 m telescope at the La Silla Observatory under programmes 099.A-9029(A) and 094.A-9012. C.E., B.M., I.R., G.M. and E.V. were supported by Spanish grant AYA 2014-55840-P; B.M., I.R., G.M. and E.V. are also supported by Spanish grant PGC2018-101950-B-100; B.M. and E.V. are also partly funded by the Spanish State Research Agency (AEI) project No. MDM-2017-0737 Unidad de Excelencia 'María de Maeztu' Centro de Astrobiología (CAB, CSIC-INTA). We thank Ana Guijarro of the Calar Alto Observatory for obtaining the CARMENES spectrum.

References

Abt, H. A. 2008, ApJS, 174, 499
Abt, H. A., & Moyd, K. I. 1973, ApJ, 182, 809
Abt, H. A., Tan, H., & Zhou, H. 1997, ApJ, 487, 365
Adamczak, J., & Lambert, D. L. 2014, ApJ, 791, 58
Arcos, C., Kanaan, S., Chávez, J., et al. 2018, MNRAS, 474, 5287
Baade, D. 1984, A&A, 135, 101
Baade, D., & Ferlet, R. 1984, A&A, 140, 72
Balona, L. A. 2000, MNRAS, 318, 289
Balona, L. A., & Ozuyar, D. 2020, MNRAS, 493, 2528
Bouchaud, K., Domiciano de Souza, A., Rieutord, M., Reese, D. R., & Kervella, P. 2020, A&A, 633, A78
Boyajian, T. S., LaCourse, D. M., Rappaport, S. A., et al. 2016, MNRAS, 457, 3988
Cataldi, G., Moór, A., Ohashi, N., et al. 2019, RNAAS, 3, 39
Cosentino, R., Lovis, C., Pepe, F., et al. 2012, in SPIE Conf. Ser., 8446, Proc. SPIE, 84461V
Cranmer, S. R. 2009, ApJ, 701, 396
David, T. J., & Hillenbrand, L. A. 2015, ApJ, 804, 146
De Rosa, R. J., Patience, J., Wilson, P. A., et al. 2014, MNRAS, 437, 1216
Eiroa, C., Rebollido, I., Montesinos, B., et al. 2016, A&A, 594, A1
Ferlet, R., Vidal-Madjar, A., & Hobbs, L. M. 1987, A&A, 185, 267
Gray, R. O., & Corbally, J., C. 2009, Stellar Spectral Classification
Hanuschik, R. W. 1995, A&A, 295, 423
Jaschek, C., & Andrillat, Y. 1998, A&AS, 130, 507
Jaschek, M., Jaschek, C., & Andrillat, Y. 1988, A&AS, 72, 505
Jaschek, M., Jaschek, C., & Andrillat, Y. 1991, A&A, 250, 127
Kambe, E., Ando, H., & Hirata, R. 1993a, A&A, 273, 435
Kambe, E., Ando, H., Hirata, R., et al. 1993b, PASP, 105, 1222
Kaufer, A., Stahl, O., Tubbesing, S., et al. 1999, The Messenger, 95, 8
Kennelly, E. J., Walker, G. A. H., & Merryfield, W. J. 1992, ApJ, 400, L71
Kennelly, E. J., Brown, T. M., Kotak, R., et al. 1998, ApJ, 495, 440
Kiefer, F., Lecavelier des Etangs, A., Augereau, J.-C., et al. 2014a, A&A, 561, L10
Kiefer, F., Lecavelier des Etangs, A., Boissier, J., et al. 2014b, Nature, 514, 462
Kiefer, F., Lecavelier des Étangs, A., Vidal-Madjar, A., et al. 2017, A&A, 608, A132
Koubsky, P., Horn, J., Harmanec, P., et al. 1993, A&A, 277, 521
Koubsky, P., Harmanec, P., Kubat, J., et al. 1997, A&A, 328, 551
Lagrange-Henri, A. M., Ferlet, R., Vidal-Madjar, A., et al. 1990, A&AS, 85, 1089
Leister, N. V., Janot-Pacheco, E., Hubert, A. M., et al. 1994, A&A, 287, 789
Manser, C. J., Gänsicke, B. T., Eggl, S., et al. 2019, Science, 364, 66
Mantegazza, L. 2000, in Astronomical Society of the Pacific Conference Series, 210, Delta Scuti and Related Stars, eds. M. Breger, & M. Montgomery, 138
Montesinos, B., Eiroa, C., Lillo-Box, J., et al. 2019, A&A, 629, A19
Quirrenbach, A., Amado, P. J., Caballero, J. A., et al. 2016, in Proc. SPIE, 9908, Ground-based and Airborne Instrumentation for Astronomy VI, 990812
Rappaport, S., Vanderburg, A., Jacobs, T., et al. 2018, MNRAS, 474, 1453
Raskin, G., van Winckel, H., Hensberge, H., et al. 2011, A&A, 526, A69
Rebollido, I., Eiroa, C., Montesinos, B., et al. 2020, A&A 639, A11
Redfield, S. 2007, ApJ, 656, L97
Rieke, G. H., Su, K. Y. L., Stansberry, J. A., et al. 2005, ApJ, 620, 1010
Rivinius, T., Štefl, S., & Baade, D. 1999, A&A, 348, 831
Rivinius, T., Carciofi, A. C., & Martayan, C. 2013, A&ARv, 21, 69
Royer, F., Zorec, J., & Gómez, A. E. 2007, A&A, 463, 671
Schrijvers, C., & Telting, J. H. 1999, A&A, 342, 453
Smette, A., Sana, H., Noll, S., et al. 2015, A&A, 576, A77
Soubiran, C., Le Campion, J.-F., Brouillet, N., & Chemin, L. 2016, A&A, 591, A118
Strøm, P. A., Bodewits, D., Knight, M. M., et al. 2020, PASP, 132, 101001
Telting, J. 2003, Ap&SS, 284, 85
Telting, J. H., & Schrijvers, C. 1997, A&A, 317, 723
Telting, J. H., Avila, G., Buchhave, L., et al. 2014, Astron. Nachr., 335, 41
van Belle, G. T. 2012, A&ARv, 20, 51
Vogt, S. S., & Penrod, G. D. 1983, ApJ, 275, 661
Walker, G. A. H., Yang, S., & Fahlman, G. G. 1987, ApJ, 320, L139
Welsh, B. Y., & Montgomery, S. L. 2018, MNRAS, 474, 1515
Welsh, B. Y., Craig, N., Crawford, I. A., & Price, R. J. 1998, A&A, 338, 674
Zorec, J., & Royer, F. 2012, A&A, 537, A120

Appendix A: Results for photospheric lines

A.1. HERMES May 2016

During the night of 2016-05-11, 20 consecutive spectra were obtained over ∼4 hours of observations. The night was not optimal and one of the spectra was not useful. Figure A.1 shows the profiles of Ca I 4226 Å and the Mg II lines obtained during this night. Several dumps and bumps lasting up to several hours are observed in both lines but seemingly not coincident. In particular, there is a depression in the Mg II line going from ∼4480 Å to 4483 Å from ∼ 2016-05-11 21h05m UT to at least 2016-05-11 23h27m UT, that is, it lasts at least ∼ 150 minutes.

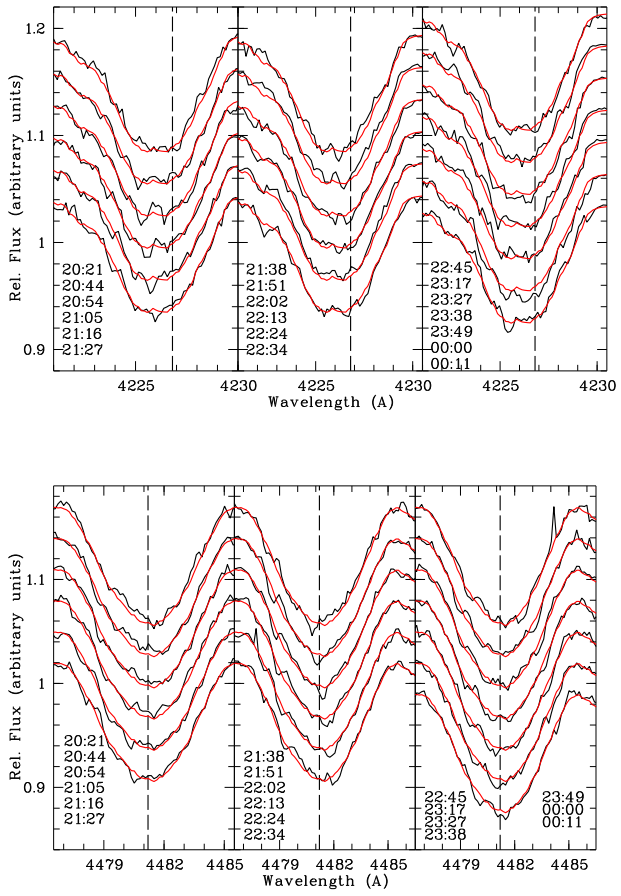

Fig. A.1. Profiles of the Ca I 4226 Å (top) and Mg II 4481 Å (bottom) lines as observed with HERMES in 2016-05-11. UTs from top to bottom and from left to right are indicated in the labels. Spectra have been rebinned to 0.1406 Å/pixel. The median of all spectra superimposed on each spectrum is plotted in red.

A.2. HERMES/FEROS from March and April 2017

During these observing runs, series spectra were taken during 12 consecutive nights as long as the air mass of the star was $\lesssim$2.0. On some nights, HERMES and FEROS spectra were obtained simultaneously and their appearance was quite similar in spite of the different spectral resolution, which provides high confidence about the reliability on the weak features seen superimposed on the line profiles. As representative results, we show below (Figs. A.2 and A.3) the spectra of the Mg II 4481 Å line on two of the nights, in one case with HERMES spectra, and one night with both HERMES and FEROS spectra:

– **2017-03-28**: During this night, 24 spectra were obtained with HERMES (two of them were not useful). Figure A.2 plots the Mg II 4481 Å line with the labels indicating the observing UT of each spectra. No obvious dumps or bumps in the line profiles that could be attributed to pulsations are clearly detected in most of the spectra, although very weak features might be present in some of them.

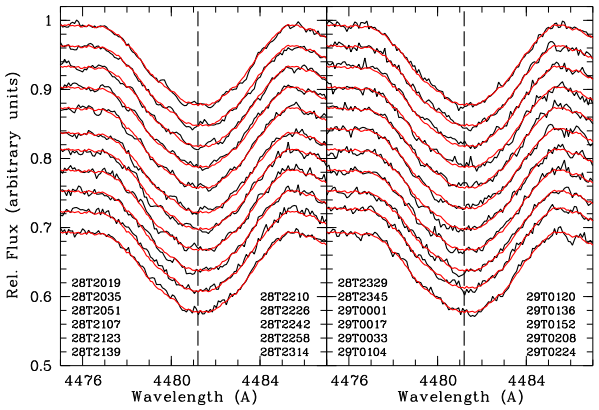

Fig. A.2. Profiles of the Mg II 4481 Å line as observed with HERMES during the night 2017-03-28/29. The spectra have been rebinned to 0.09 Å/pixel; the median of the night is plotted in red superimposed on each spectrum. In both panels, UTs from top to bottom and from left to right correspond to spectra ordered from top to bottom.

– **2017-04-01/02**: On this night, 21 HERMES and 28 FEROS spectra were taken along a time interval of ∼9.5 hours. Figure A.3 plots the Mg II 4481 Å line of these spectra. Several features, mostly dumps, are distinctly present in the spectra, although no obvious features are discernible in some of them (e.g. the spectra taken at 2017-04-02 04h23m UT or 2017-04-02 04h28m UT). We note that some features appear on the blue side of the line profile but do not always apparently propagate to the red wing. It is noticeable that the HERMES and FEROS spectra agree very well; see for example the spectra taken at 2017-04-02 01h44m UT and 2017-04-02 01h45m UT with HERMES and FEROS respectively, or the ones taken at 2017-04-02 02h32m UT with both HERMES and FEROS simultaneously.

Appendix B: Results for non-photospheric lines

B.1. HERMES March 2017

During this period, HERMES spectra were taken over eight consecutive nights. Figure B.1 shows the median spectra corresponding to each night of Ca II K and Fe II 5169 Å, as well as the spectra obtained during the night 2017-03-10. Variability is observed in a daily basis and in consecutive spectra of a single night. Note that the changes of Ca II and Fe II are different, and that the 3 km/s emission is not distinguishable in some spectra.

B.2. FEROS 2017 April

During this period, FEROS spectra were taken over nine consecutive nights. Figure B.2 shows the median spectra of all nights

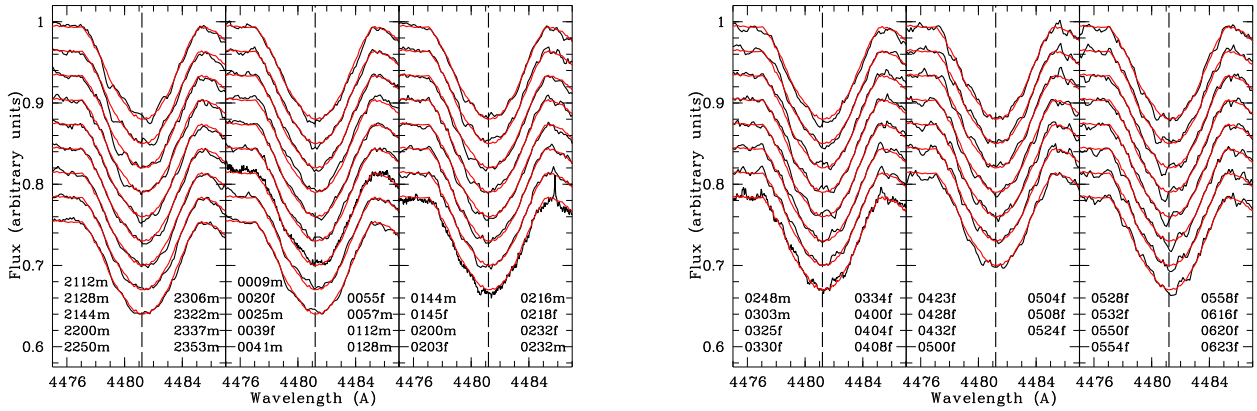

Fig. A.3. Profiles of the Mg II 4481 Å line as observed with HERMES and FEROS during the night of 2017-04-01/02 along ~9:30 hours. All spectra have been rebinned to 0.12 Å/pixel, and the median of the night is plotted in red superimposed on each spectrum. Spectra with 'm' in the labels refer to those obtained with HERMES and those with 'f' refer to FEROS. Labels correspond to spectra from top to bottom and then the two columns from left to right.

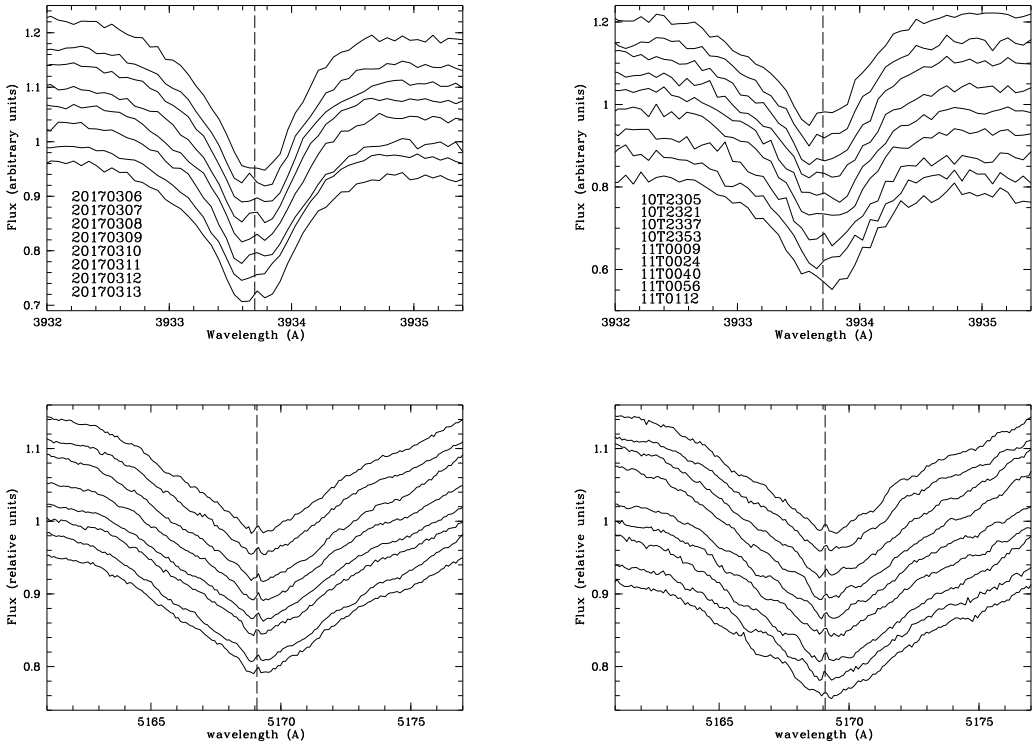

Fig. B.1. Left: Nightly median of Ca II K and Fe II 5169 Å. Dates are indicated in the labels. Right: Some consecutive spectra taken during the night 2017-03-10/11. Exposure time of each spectrum is 15 minutes. The resolution of the Ca II spectra is is 0.0625 Å/pixel, while for Fe II is 0.0938 Å/pixel. Ca II K shows variability from night to night as well as irregular short timescale variability in individual nights. The central emission is seen in some of the nights, and both blue- and red-shifted minima change their relative strength. With respect to the Fe II line the central emission is present in all nights but the variability is less pronounced than the one in the K line and no correlation is seen.

corresponding to Ti II 3759 and 3761 Å, Ca II K, and Fe II 5169 Å. We note that the ~3 km s^{-1} emission is observed on all nights and that the variations are different from line to line.

Appendix C: Observing Log

Table C.1 is only available in electronic form at the CDS.

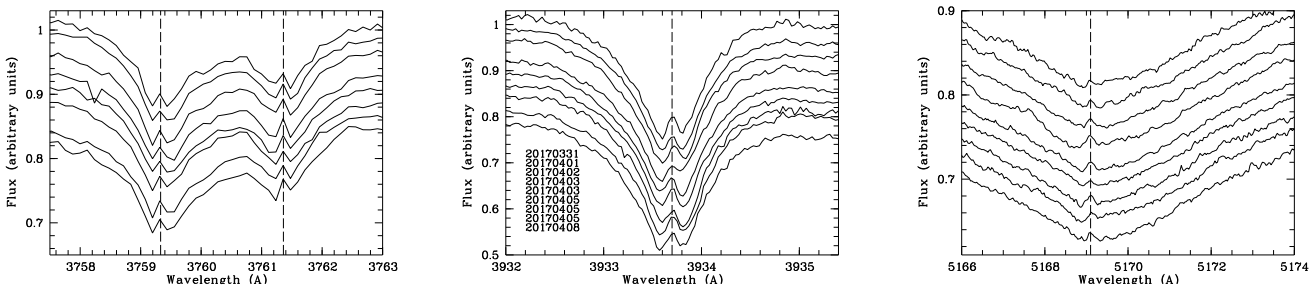

Fig. B.2. Nightly median of Ti II 3759 and 3761 Å, Ca II K and Fe II 5169 Å lines as observed from 2017-03-31 to 2017-04-08 with FEROS. Dates are indicated from top to bottom in the Ca II K panel.